doi: 10.82124/CEAS-GNC-2026-XYZ CEAS-GNC-2026-XYZ

Anti-Windup Flight Control Design for Agile Aerospace Vehicles

Igor Pszczolkowski Delft University of Technology, 2629HS, Delft, The Netherlands. igorpszcz@gmail.com

Elmar Wallner MBDA Deutschland GmbH, 86529, Schrobenhausen, Germany. elmar.wallner@mbda-systems.de

Sebastian Fleishmann MBDA Deutschland GmbH, 86529, Schrobenhausen, Germany. sebastian.fleishmann@mbda-systems.de

Spilios Theodoulis Associate Professor, Delft University of Technology, 2629HS, Delft, The Netherlands. S.Theodoulis@tudelft.nl

ABSTRACT

This paper describes a flight control design method for agile aerospace vehicle applications subject to rate saturation constraints. The model includes linear airframe dynamics and a second order nonlinear actuator. A baseline controller is synthesized utilizing the signal-based closed-loop shaping design method to obtain good performance and robustness metrics in the linear domain. Design of an Anti-Windup augmentation based on the rate saturation signal is then carried out to address the performance degradation of a constrained system. Three distinct Anti-Windup schemes are analyzed, ranging from classical to modern frameworks. A comparative analysis of the proposed compensators is provided by evaluating the $\mathcal{L}_2$ gain and simulating a flight scenario under a nonlinear actuator with multiple saturations. All analyzed Anti-Windup schemes reduce the upper bound on the $\mathcal{L}_2$ gain of the system and show a significant improvement in disturbance rejection response.

Keywords: Anti-Windup; Robust Control; H-infinity; Actuator Saturation

Nomenclature

α = Angle of Attack
δ = Fin Deflection
θ = Pitch Angle
ζ = Damping Ratio
ω = Natural Frequency
q = Pitch Rate

1 Introducion

The agile aerospace vehicle control problem is challenging due to fast dynamics, wide flight envelopes, and actuator saturation. These factors demand controllers robust to aerodynamic uncertainties and nonlinearities, ensuring stability and performance, which are often mission-critical.

Advances in robust control now allow fixed-structure designs [1, 2], increasing the applicability of $\mathcal{H}_\infty$ methods to aerospace autopilots, including Closed-loop Shaping (CLS) [3–5], Open-loop Shaping (OLS) [6–8], and more recently, signal-based design via `systune` [9, 10]. However, these methods often neglect actuator saturation, which can severely degrade performance.

Anti-Windup (AW) augmentation addresses this issue, with early schemes unified in [11] and extended through sector-condition analysis [12], stability domain maximization, and $\mathcal{L}_2$ gain minimization [13]. Notable frameworks include Direct Linear AW (DLAW) [14, 15] and Model Recovery AW (MRAW) [16–18], with systematic descriptions in [19–21]. Despite this, literature comparisons between AW schemes remain scarce, with recent exceptions in guided systems applications [22, 23].

While AW techniques typically address magnitude saturation, the rate saturation, known to induce pilot-induced oscillations [24, 25], has received less attention. Extensions for rate limits require reformulated models [26, 27], and few works treat both magnitude and rate limits [28, 29]. Acceleration saturation is even less studied, with [30] being a rare example.

This paper applies robust control and AW augmentation to design a baseline controller with multiple AW compensators, comparing their performance via $\mathcal{L}_2$ gain analysis and demanding simulations. The baseline controller is synthesized using CLS, and AW methods range from classical to modern DLAW and MRAW frameworks. The paper is organized as follows: section 2 covers flight dynamics modeling; section 3 details the baseline controller design; section 4 presents AW augmentation; and section 5 compares performance and robustness across control schemes.

2 Flight Dynamics Modeling

This section discusses the modeling of the agile aerospace vehicle, including the longitudinal dynamics of the airframe, and the linear and nonlinear actuator models used in design and subsequent simulations. Modeling aspects of the rate saturation are also discussed, including the method of recasting the system into a standard form, necessary for anti-windup design.

2.1 Airframe

The notional model of an airframe considered for this research work represents the longitudinal dynamics of an agile aerospace vehicle, which are controlled using movable aerodynamic surfaces. State vector consists of angle of attack, pitch angle, and pitch rate, and is defined as $x_p = [\alpha\ \theta\ q]^T$. Input to the airframe dynamics is the actuator deflection $u_p = \delta$. It is assumed that perfect measurements of pitch angle and pitch rate are available, defining the airframe output vector as $y = [\theta\ q]^T$. The resulting state-space system, denoted by $G(s)$, is given by Equation 1. This study considers a single flight point, hence, the aerodynamic coefficients assume fixed values.

$$\begin{bmatrix} \dot{\alpha} \\ \dot{\theta} \\ \dot{q} \end{bmatrix} = \begin{bmatrix} Z_\alpha & 0 & Z_q \\ 0 & 0 & 1 \\ M_\alpha & 0 & M_q \end{bmatrix} \begin{bmatrix} \alpha \\ \theta \\ q \end{bmatrix} + \begin{bmatrix} Z_\delta \\ 0 \\ M_\delta \end{bmatrix} \begin{bmatrix} \delta \end{bmatrix}$$
$$\begin{bmatrix} \theta \\ q \end{bmatrix} = \begin{bmatrix} 0 & 1 & 0 \\ 0 & 0 & 1 \end{bmatrix} \begin{bmatrix} \alpha \\ \theta \\ q \end{bmatrix} + \begin{bmatrix} 0 \\ 0 \end{bmatrix} \begin{bmatrix} \delta \end{bmatrix} \tag{1}$$

2.2 Linear Actuator

The actuator model is of high importance for this study, as the saturation limit values and their implementation are one of the actuator characteristics. Linear dynamics of the actuator are given by Equation 2. Input to actuator dynamics is the commanded deflection angle δ_{cmd}, and the output is the actual deflection angle δ. The dynamics represent the system responsible for the movement of aerodynamic control surfaces, eg, an electro-mechanical servo.

$$A(s) = \frac{\omega_a^2}{s^2 + 2\zeta_a\omega_a + \omega_a^2} \tag{2}$$

2.3 Saturated Actuator

While the linear actuator can be used within the design model, ultimately, the performance will be evaluated on a nonlinear actuator model. Its implementation in Simulink is presented in Figure 1. Four saturation elements are present in the diagram, as magnitude saturation is limited both at the input and at the output. Input limitation guarantees that no commands exceeding the limits will be passed to the actuator dynamics, while output limitation models the physical limits of the actuator, for example a mechanical stop. Limited integrators are chosen to model the rate and output magnitude saturations. The feedback connection represents a state reset condition, which ensures that, when magnitude saturation is reached, the rate drops to zero, corresponding to the real-world behavior of a system with nested saturations. Additionally, a saturation on acceleration without a limited integrator is included.

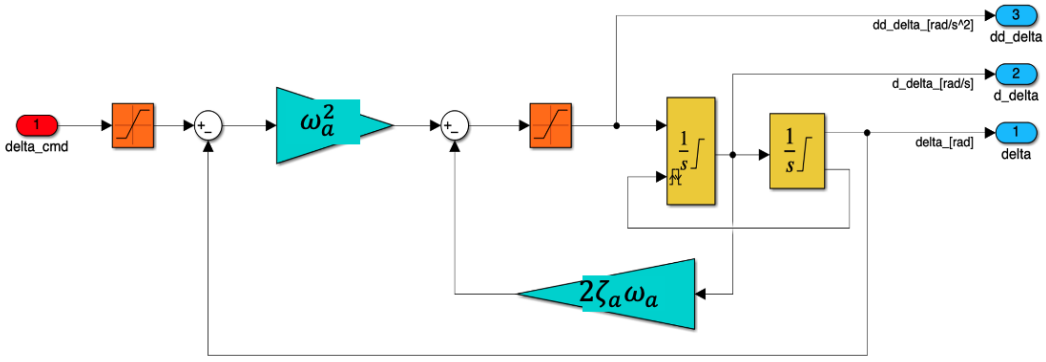

Fig. 1 Nonlinear actuator model in Simulink

2.4 Rate Saturation Modeling

This work focuses on rate saturation constraints. Since full access to nonlinear actuator states is assumed unavailable, the rate saturation block must be isolated to extract the deadzone signal, requiring a reformulation where the rate signal is accessible. The rate is approximated as $\frac{s}{cs+1}$, with c linked to the

sampling rate. To avoid added lag, the modification from [26] is adopted, introducing a loop with free parameter K to recover the unconstrained response when saturation is inactive. As noted in [26] and [27], K is chosen as a trade-off between response recovery and numerical stability in LMI-based AW synthesis. The equivalent system, shown in Figure 2, is the closed-loop of a new plant $\mathscr{G}(s)$ and controller $\mathscr{K}(s)$. The input to the saturation block is the commanded control rate $\dot{\delta}_{cmd}$, enabling analysis and AW design for rate saturation. The new plant state vector is $\bar{x}_p = [x_p; \delta_{cmd}]^T$, and the plant output (equivalently controller input) is $\bar{y} = [y; \delta_{cmd}]^T = \bar{u}_c$.

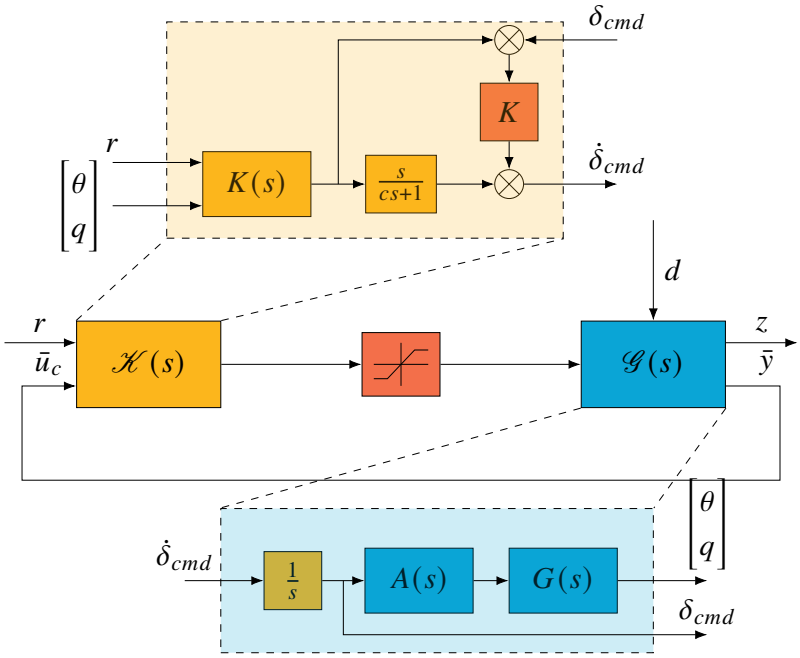

Fig. 2 Equivalent closed-loop system with plant and controller details

Controller matrices are also reformulated, so that the new controller output is now $\bar{y}_c$. Assuming that a controller with state-space realization $(A_c, B_{cu}, B_{cr}, C_c, D_{cu}, D_{cr})$ has been designed, the new controller state-space matrices can be formulated as given in Equation 3.

$$\left[\begin{array}{c|c|c} \bar{A}_c & \bar{B}_{cu} & \bar{B}_{cr} \\ \hline \bar{C}_c & \bar{D}_{cu} & \bar{D}_{cr} \end{array}\right] = \left[\begin{array}{c|cc|c} A_c & B_{cu} & 0 & B_{cw} \\ \hline KC_c + C_cA_c & C_cB_{cu} & -K & C_cB_{cw} \end{array}\right] \tag{3}$$

3 Flight Control Design

Firstly, the baseline flight control design is carried out. This section defines the main control objectives and the control structure used in this work. The chosen control design methodology is the signal-based $\mathcal{H}_\infty$ CLS design, for which the tuning goals and relevant transfer functions are detailed at the end of the section.

3.1 Control Objectives

Control objectives for this work largely follow the methodology presented in [10], although not every requirement discussed in this work will be incorporated. The key goal is to achieve good disturbance rejection in the linear domain. Achieving it will create a baseline for designing the anti-windup augmentation and extending the controller to nonlinear domain. The main top-level control requirements can be summarized as follows:

(L1) Disturbance Rejection: Closed-loop system shall be able to reject disturbances at the plant input and output.

(L2) Reference Tracking: Closed-loop system shall be able to track a reference signal with no steady-state error.

(L3) Stability Margins: Stability margins at plant input and plant output, for both loop-at-a-time and multi-loop cases, shall be sufficiently high.

(L4) Control Action Minimization: Performance objectives of disturbance rejection and reference tracking shall be achieved with minimum control action.

3.2 Control Structure

The control structure in this work takes inspiration from [31], with a key difference that measured signals are θ and q, instead of n_z and q. It resembles a classical PID with an integral gain on the tracking error, proportional gains on two measured signals, and a feed-forward gain on the reference signal. This architecture forms a control law given by Equation 4. The controller input is the measured output of the plant $u_c = [\theta\ q]^T$, while the output is the commanded deflection $y_c = \delta_{cmd}$.

$$\delta_{cmd} = K_i \int (\theta - \theta_{ref})dt + K_\theta \theta + K_q q + K_{ff}\theta_{ref} \tag{4}$$

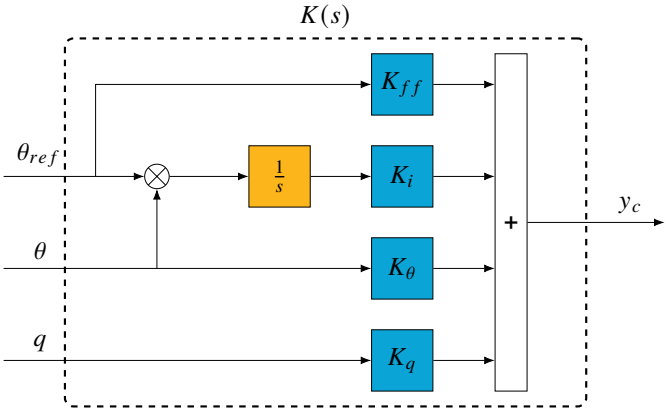

Fig. 3 Control structure block diagram

3.3 Signal-Based $\mathcal{H}_\infty$ CLS Design

Now a controller will be synthesized such as to satisfy the broad objectives set out in subsection 3.1, while adhering to the control structure defined in subsection 3.2. The plant $\widehat{G}$, formed by connecting the linear actuator and the airframe dynamics in series, and the controller K, form a closed-loop system. The closed-loop system $(\widehat{G}, K)$, denoted from now on as P_{cl}, has a state-space representation given by Equation 5, with state vector $x_{cl} = [x_p\ x_c]^T \in \mathbb{R}^{n_p+n_c}$, and performance output vector $z = y = [\theta\ q]^T \in \mathbb{R}^{n_z}$. Additional details about the matrices below can be found in Appendix A.

$$P_{cl}: \begin{cases} \dot{x}_{cl} = \mathbf{A}x_{cl} + \mathbf{B_d}d + \mathbf{B_r}r \\ z = \mathbf{C_z}x_{cl} + \mathbf{D_{zd}}d + \mathbf{D_{zr}}r \\ y_c = \mathbf{C_y}x_{cl} + \mathbf{D_{yd}}d + \mathbf{D_{yr}}r \end{cases} \tag{5}$$

Design methodology adopted in this work follows general principles of $\mathcal{H}_\infty$ CLS design, which involves shaping the desired closed-loop transfer functions in the frequency domain. The main control

objective is disturbance rejection, therefore, a 4-block approach is chosen [32], which can guarantee disturbance rejection at both plant inputs and outputs.

General expressions for n-th order weighting filters W_1 (low-pass) and W_2 (high-pass) are given by equations (6a) and (6b), respectively. The filters are completely characterized by their low-frequency gain A, high-frequency gain M, and crossover frequency ω^*. Given these values. they are constructed with MATLAB's `makeweight` function.

$$W_1(s) = \left(\frac{s + \omega_1^* A_1^{\frac{1}{n}}}{\left(\frac{1}{M_1}\right)^{\frac{1}{n}} s + \omega_1^*} \right)^n \tag{6a}$$

$$W_2(s) = \left(\frac{A_2^{\frac{1}{n}} s + \omega_2^*}{s + \omega_2^* \left(\frac{1}{M_2}\right)^{\frac{1}{n}}} \right)^n \tag{6b}$$

For output sensitivity $S_{o,\theta}$, low values are desired in the low frequency range. Desired high frequency gain can be linked to phase margin via $M_{S_{o,\theta}} \leq 1/2 \sin(PM/2)$. The crossover frequency is desired within a close range of the airframe frequency poles. For control sensitivity $KS_{o,\theta}$, the crucial parameter is the desired crossover frequency, as attenuation is desired beyond the natural frequency of the actuator. Gains at low and high frequencies are not as relevant for this function, as long as they are chosen as high and low values, respectively. The desired shape for input co-sensitivity T_i is approximately an inverse of output sensitivity, with low values desired at high frequencies, and the low-frequency gain linked to phase margin. For plant sensitivity $S_{o,\theta}G$, the desired behavior at low frequencies is very similar to that of output sensitivity, while at high frequencies, the function will follow the open-loop gain of the plant; therefore, constraining it there is not necessary.

To improve the tuning, a second order reference model is constructed, given by Equation 7. Model following constraint is also implemented as an $\mathcal{H}_\infty$ constraint, with a new weighting filter defined. The aim is to minimize the error in pitch angle, e_θ, between the reference model and the actual model responses. Desired shape in the frequency domain involves low values at low frequencies to guarantee minimal error within the model's bandwidth.

$$G_{ref}(s) = \frac{\omega_{ref}^2}{s^2 + 2\zeta_{ref}\omega_{ref} + \omega_{ref}^2} \tag{7}$$

3.4 CLS Controller Synthesis

To carry out the controller synthesis all the requirements are aggregated and translated into optimization goals. Synthesis is performed using MATLAB's `systune`, specifying the five established weighting filters as hard constraints, utilizing the `TuningGoal.Gain` function. Additionally, disk margins are introduced as soft constraints with `TuningGoal.Margins`. The optimization problem is solved with `systune`, utilizing many random starts to avoid local minima. Resulting singular value plots can be seen in Figure 4. The most constraining requirements are those put on output sensitivity $S_{o,\theta}$, control sensitivity $KS_{o,\theta}$, and model following M. This is largely due to a very fast reference model being chosen. For the output sensitivity, the peak is bounded, which indicates satisfactory margins, while the achieved crossover frequency almost coincides with the crossover frequency of the weighting filter.

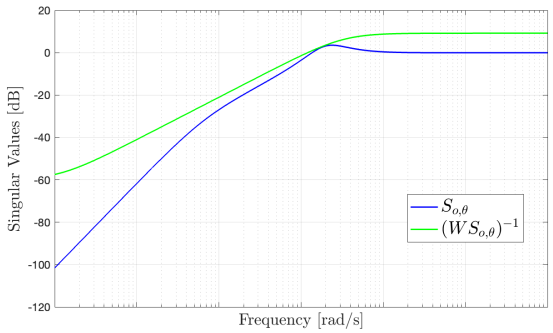

(a) Output Sensitivity $S_{o,\theta}$

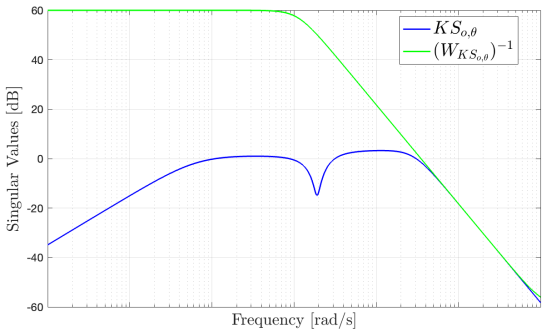

(b) Control times Sensitivity $KS_{o,\theta}$

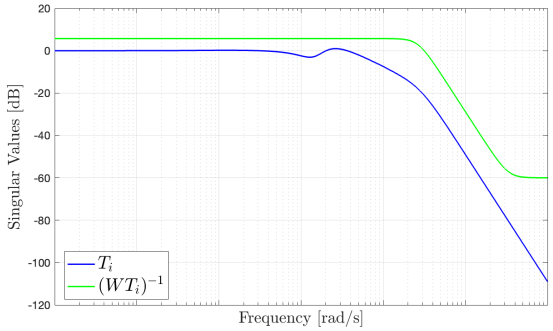

(c) Input Co-Sensitivity T_i

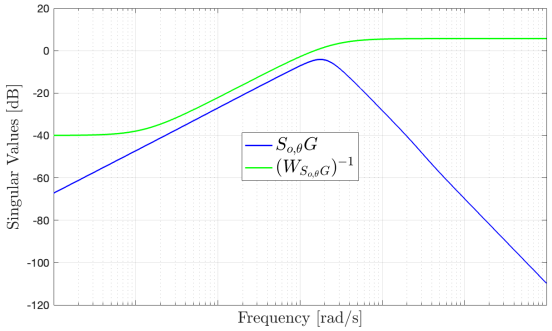

(d) Sensitivity times plant $S_{o,\theta}G$

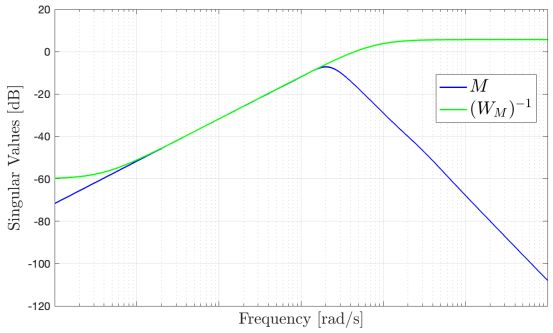

(e) Model following M

Fig. 4 Shaped closed-loop transfer functions resulting from signal-based $\mathcal{H}_\infty$ CLS controller design, along with corresponding weighting filters

4 Anti-Windup Design

Anti-Windup design is motivated by the need to address the performance and stability degradation caused by introducing saturation nonlinearities into the system. This section aims to present various methods of synthesis and analysis of AW augmentation. The main objectives and possible structure of anti-windup compensation are detailed. The formulation and synthesis method for three distinct anti-windup schemes are presented, highlighting their main aspects.

4.1 Anti-Windup Objectives

It was shown that even a controller with good performance and robustness measures, designed in the linear domain, can struggle when exposed to saturation nonlinearities. To perform AW design, a new set of objectives is defined, taken from [20].

- **(A1) Small Signal Preservation:** To make the response of the anti-windup augmented closed-loop system match the response of the unconstrained closed-loop system whenever possible
- **(A2) Asymptotic Stability:** To make, in the absence of exogenous inputs, a desired constant operating point asymptotically stable with a basin of attraction at least as big as the set of states over which the system is expected to operate
- **(A3) Input-Output Stability:** To induce a bounded response for initial states and exogenous input that are expected during operation
- **(A4) Unconstrained Response Recovery:** To recover the unconstrained closed-loop response asymptotically whenever possible

(A1) essentially means that the AW closed-loop system should match the unconstrained system's response in regions where the saturation equals the identity. In this work, fulfilling **(A1)** involves selecting a rate saturation model that has negligible influence in the linear region, as discussed in subsection 2.4. **(A2)** and **(A3)** can be quantified using performance measures such as the domain of attraction $\mathcal{E}(P)$ or the $\mathcal{L}_2$ gain from disturbances to outputs. Since the plant is stable and the vehicle faces significant external disturbances, the designs here emphasize **(A3)**. **(A4)** reflects an MRAW design philosophy, but it will be assessed solely through time-domain simulations.

4.2 General Anti-Windup Structure

General structure for linear AW design is a standard interconnection, where a saturation block driving the AW scheme is isolated between the plant and the controller. where . Two distinct architectures can be identified: full-authority AW, where the signal is injected directly into the controller (Figure 5a); and external AW, where the signals are injected into the controller's input and output (Figure 5b). The full-authority architecture requires access to the controller states.

This structure describes both anti-reset windup and static DLAW, which are similar for low-order controllers. These schemes use the full-authority AW architecture, which assumes direct availability of the controller states. The designs are also static, which reduces the AW design problem to computing D_{aw}.

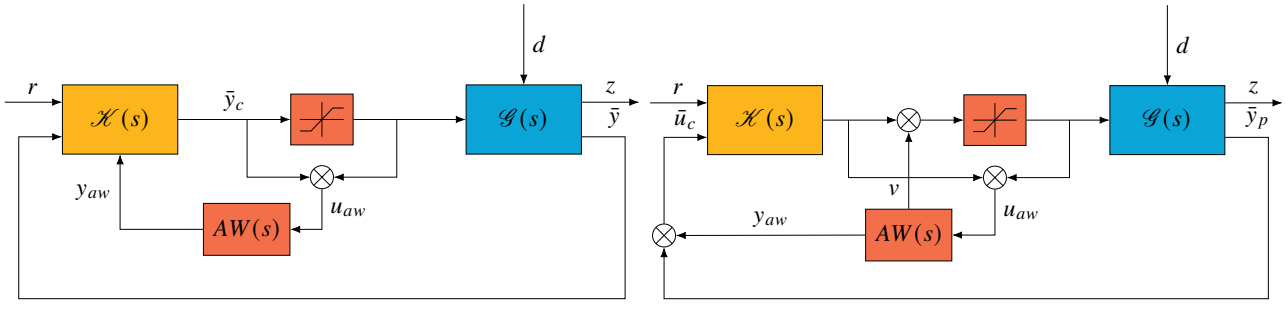

(a) Closed-loop system for AW design with full-authority architecture

(b) Closed-loop system for AW design with external architecture

Fig. 5 Comparison of different AW compensation architectures

$\mathscr{G}(s)$ is the extended plant model defined in subsection 2.4. The block $\mathscr{K}(s)$ represents the linear controller, designed in section 3, extended by parts of the rate saturation model, as shown in subsec-

tion 2.4. The state-space form of the controller, taking into account both previous linear design and the rate saturation modeling, is given by Equation 8. Control gains used as a baseline for AW design are the gain of the linear controller, as the AW compensator is intended as an a posteriori augmentation.

$$\mathscr{K}: \begin{cases} \dot{\bar{x}}_c = \bar{A}_c \bar{x}_c + \bar{B}_{cu} \bar{u}_c + \bar{B}_{cr} r + v_1 \\ \bar{y}_c = \bar{C}_c \bar{x}_c + \bar{D}_{cu} \bar{u}_c + \bar{D}_{cr} r + v_2 \end{cases} \tag{8}$$

4.3 Anti-Windup Methods Overview

This paper will present a comparison between three different AW schemes. The first one, Anti-Reset windup (AR), is a classical AW method [11], featuring a single AW gain. The second method, which falls under the framework of the Direct Linear Anti-Windup (DLAW) [14, 15], is an extension of AR acting on all the controller states and outputs. Both of these methods only involve static compensators, use full-authority architecture, and will be synthesized by minimizing the $\mathcal{L}_2$ gain from disturbance inputs to performance outputs.

The third method provides an alternative design framework, as it follows the objective of recovering the response of an unconstrained plant, based on an online plant model. Such methods are referred to as Model-Recovery Anti-Windup (MRAW), and are generally described with external architecture. The method featured in this work uses a dynamic compensator synthesized by minimizing a quadratic performance index [17]. A brief comparison of key aspects of the methods is given in Table 1.

Table 1 Overview of AW compensators

	AW Schemes		
	AR	**DLAW**	**MRAW**
Static/Dynamic	Static	Static	Dynamic
Injection Type	Full-authority	Full-authority	External
No. of AW Gains	1	3 ($n_c + n_u$)	6 (n_p)
Synthesis Method	$\mathcal{L}_2$ Gain	$\mathcal{L}_2$ Gain	LQ-based

4.4 AR & DLAW Formulation

Before conducting AW synthesis it is crucial to formulate the expression for the closed-loop AW system $\mathbb{P}_{cl}$, so that the expressions for design LMIs can follow. Equation 9 provides the state-space equations for $\mathbb{P}_{cl}$. In the equation below, ϕ_r represents the rate deadzone. This formulation is valid for static AW compesantors, encapsulating the AR and DLAW methods.

$$\mathbb{P}_{cl}: \begin{cases} \dot{x}_{cl,aw} = \mathbb{A} x_{cl,aw} + (\mathbb{B}_\phi + \mathbb{B}_v D_{aw}) \phi_r(\bar{y}_c) + \mathbb{B}_d d + \mathbb{B}_r r \\ z = \mathbb{C}_z x_{cl,aw} + (\mathbb{D}_{z\phi} + \mathbb{D}_{zv} D_{aw}) \phi_r(\bar{y}_c) + \mathbb{D}_{zd} d + \mathbb{D}_{zr} r \\ \bar{y}_c = \mathbb{C}_y x_{cl,aw} + (\mathbb{D}_{y\phi} + \mathbb{D}_{yv} D_{aw}) \phi_r(\bar{y}_c) + \mathbb{D}_{yd} d + \mathbb{D}_{yr} r \end{cases} \tag{9}$$

Closed-loop matrices are expressed in terms of new plant and controller matrices according to Equation 10. The AW injection matrices $\mathbb{B}_v$, $\mathbb{D}_{zv}$, and $\mathbb{D}_{yv}$ are not included below, as they are determined by the choice between AR and DLAW, and are detailed in Table 2.

$$\left[\begin{array}{c|c|c|c} \mathbb{A} & \mathbb{B}_\phi & \mathbb{B}_d & \mathbb{B}_r \\ \hline \mathbb{C}_z & \mathbb{D}_{z\phi} & \mathbb{D}_{zd} & \mathbb{D}_{zr} \\ \hline \mathbb{C}_y & \mathbb{D}_{y\phi} & \mathbb{D}_{yd} & \mathbb{D}_{yr} \end{array}\right] = \left[\begin{array}{cc|c|cc} \bar{A}_p + \bar{B}_{pu}\bar{D}_{cu}\bar{C}_p & \bar{B}_{pu}\bar{C}_c & \bar{B}_{pu} & \bar{B}_{pd} + \bar{D}_{pd}\bar{D}_{cu}\bar{B}_{pu} & \bar{D}_{cr}\bar{B}_{pu} \\ \bar{B}_{cu}\bar{C}_p & \bar{A}_c & 0 & \bar{D}_{pd}\bar{B}_{cu} & \bar{B}_{cr} \\ \hline \bar{C}_p & 0 & 0 & \bar{D}_{pd} & 0 \\ \hline \bar{D}_{cu}\bar{C}_p & \bar{C}_c & 0 & \bar{D}_{cu}\bar{D}_{pd} & \bar{D}_{cr} \end{array}\right] \tag{10}$$

The AW compensator is represented by a matrix D_{aw}, which can be partitioned as in Equation 11 to differentiate between signals added to controller states ($D_{aw,1}$), and signals added to controller outputs ($D_{aw,2}$). For the AR method, only the signal $v_{1,1}$ is considered, which reduces the matrix to a single gain $D_{aw} \in \mathbb{R}$. Considering the structure of $\mathscr{K}(s)$, this corresponds to only acting on the integrator state of the controller.

$$D_{aw} = \left[\frac{D_{aw,1}}{D_{aw,2}}\right] \Rightarrow y_{aw} = \left[\begin{array}{c} v_{1,1} \\ \hline v_{1,2} \\ \hline v_2 \end{array}\right] \tag{11}$$

DLAW method involves signals acting on both controller states and controller. Therefore, the AW matrix features a separate gain for each controller state and output, resulting in $D_{aw} \in \mathbb{R}^{(n_c+n_u)\times n_u}$. It should be noted that an AW signal is injected directly into the controller output, after only passing through a static gain block. This creates a risk of an algebraic loop and an ill-posed system, which has to be addressed during the synthesis of this structure.

4.5 MRAW Formulation

The same process of formulating an expression for a closed-loop system can be repeated for MRAW. The new closed-loop AW system $\mathcal{P}_{cl}$ is given by Equation 12, with new notation introduced to easier differentiate the various schemes.

$$\begin{cases} \dot{x}_{cl,aw} = \mathcal{A}x_{cl,aw} + \mathcal{B}_\phi\phi_r(\bar{y}_c) + \mathcal{B}_d d + \mathcal{B}_r r \\ z = C_z x_{cl,aw} + \mathcal{D}_{z\phi}\phi_r(\bar{y}_c) + \mathcal{D}_{zd} d + \mathcal{D}_{zr} r \\ \bar{y}_c = C_y x_{cl,aw} + \mathcal{D}_{y\phi}\phi_r(\bar{y}_c) + \mathcal{D}_{yd} d + \mathcal{D}_{yr} r \end{cases} \tag{12}$$

Specific matrices from the above closed-loop system equations are expanded in Equation 13. For compactness, the formulation uses definitions given in Equation 9, as the main differences lie in extending the AW compensator to a dynamic system, thus introducing new AW matrices (A_{aw}, B_{aw}, C_{aw}). It is convenient to establish a state-space representation of this scheme consistent with the previous framework, so that the same tools can be used for analysis.

$$\left[\begin{array}{c|c|c|c} \mathcal{A} & \mathcal{B}_\phi & \mathcal{B}_d & \mathcal{B}_r \\ \hline C_z & \mathcal{D}_{z\phi} & \mathcal{D}_{zd} & \mathcal{D}_{zr} \\ \hline C_y & \mathcal{D}_{y\phi} & \mathcal{D}_{yd} & \mathcal{D}_{yr} \end{array}\right] = \left[\begin{array}{cc|c|c|c} \mathbb{A} & \mathbb{B}_v C_{aw} & \mathbb{B}_\phi + \mathbb{B}_v D_{aw} & \mathbb{B}_d & \mathbb{B}_r \\ 0 & A_{aw} & B_{aw} & 0 & 0 \\ \hline \mathbb{C}_z & \mathbb{D}_{zv} C_{aw} & \mathbb{D}_{z\phi} + \mathbb{D}_{zv} D_{aw} & \mathbb{D}_{zd} & \mathbb{D}_{zr} \\ \hline \mathbb{C}_y & \mathbb{D}_{yv} C_{aw} & \mathbb{D}_{y\phi} + \mathbb{D}_{yv} D_{aw} & \mathbb{D}_{yd} & \mathbb{D}_{yr} \end{array}\right] \tag{13}$$

The AW matrices can be expressed in terms of the plant state-space matrices, and a gain matrix $K_{aw} \in \mathbb{R}^{n_u \times n_p}$, which will be tuned as part of MRAW synthesis. The AW matrices of the complete compensator are given in Equation 14.

$$\left[\begin{array}{c|c} A_{aw} & B_{aw} \\ \hline C_{aw} & D_{aw} \end{array}\right] = \left[\begin{array}{c|c} \bar{A}_p + \bar{B}_{pu} K_{aw} & \bar{B}_{pu} \\ \hline \bar{C}_p & 0 \\ K_{aw} & 0 \end{array}\right] \tag{14}$$

Finally, the AW injection matrices $\mathbb{B}_v, \mathbb{D}_{zv}, \mathbb{D}_{yv}$ are presented for all schemes in Table 2 to allow for easier comparison. These matrices describe the connection between the AW compensator block and the controller, thus completing the definition of the system and allowing us to proceed to AW compensator synthesis.

Table 2 Overview of AW injection matrices

		AW Schemes		
		AR	**DLAW**	**MRAW**
AW Matrices	$\mathbb{B}_v$	$\begin{bmatrix} 0_{n_p \times n_u} \\ 1 \\ 0 \end{bmatrix}$	$\begin{bmatrix} 0_{n_p \times n_c} & \bar{B}_{pu} \\ I_{n_c} & 0_{n_c \times n_u} \end{bmatrix}$	$\begin{bmatrix} \bar{B}_{pu}\bar{D}_{cu} & \bar{B}_{pu} \\ \bar{B}_{cu} & 0_{n_c \times n_u} \end{bmatrix}$
	$\mathbb{D}_{zv}$	$\begin{bmatrix} 0 \end{bmatrix}$	$\begin{bmatrix} 0_{n_u \times n_z} \end{bmatrix}$	$\begin{bmatrix} 0_{n_u \times n_z} \end{bmatrix}$
	$\mathbb{D}_{yv}$	$\begin{bmatrix} 0 \end{bmatrix}$	$\begin{bmatrix} 0_{n_u \times n_c} & I_{n_u} \end{bmatrix}$	$\begin{bmatrix} \bar{D}_{cu} & I_{n_u} \end{bmatrix}$

4.6 $\mathcal{L}_2$-Based Design with LMIs

This method of AW compensator synthesis aims to fulfill **(A3)**, and thus to minimize the $\mathcal{L}_2$ gain from disturbance inputs to performance outputs. By minimizing the $\mathcal{L}_2$ gain one can achieve a bound on how much a given disturbance can amplify a chosen output, when a specific AW scheme is included in the closed-loop system. The $\mathcal{L}_2$ gain can be expressed as a minimum γ, for a given bound on the energy of the disturbance signal, denoted by s, such that Equation 15 holds.

$$||z||_2 \leq \gamma ||d||_2 \quad \forall d \text{ s.t. } ||d||_2 \leq s \tag{15}$$

Synthesizing the optimal AW compensator is now equivalent to minimizing γ, while finding matrices $Q \in \mathbb{R}^{(n_p+n_c)\times(n_p+n_c)}$, $U \in \mathbb{R}^{n_u}$, $Y \in \mathbb{R}^{n_u \times (n_p+n_c)}$ and $X \in \mathbb{R}^{(n_c+n_u)\times n_u}$, such that the LMI conditions in Equation 16 hold. This formulation is analogous to the one used in [27], with the addition of a free variable X to incorporate the AW compensator gains into the synthesis.

$$
\begin{aligned}
&\min_{Q,U,Y,X,\gamma} \gamma \quad \text{subject to} \\
&Q = Q^T > 0 \\
&U > 0 \\
&\mathrm{He}\begin{bmatrix} \mathbb{A}Q & \mathbb{B}_\phi U + \mathbb{B}_v X & \mathbb{B}_d & 0 \\ Y + \mathbb{C}_y Q & \mathbb{D}_{y\phi} U - U + \mathbb{D}_{yv} X & \mathbb{D}_{yd} & 0 \\ 0 & 0 & -\frac{I}{2} & 0 \\ \mathbb{C}_z Q & \mathbb{D}_{z\phi} U + \mathbb{D}_{zv} X & \mathbb{D}_{zd} & -\frac{\gamma^2 I}{2} \end{bmatrix} < 0 \\
&\begin{bmatrix} Q & Y^T \\ Y & \frac{\bar{u}^2}{s^2} \end{bmatrix} \geq 0 \\
&\mathrm{He}\begin{bmatrix} (\rho - 1)U - \rho(U\mathbb{D}_{y\phi} + X\mathbb{D}_{yv}) & \rho\mathbb{D}_{yv} X \\ \rho U \mathbb{D}_{y\phi} & \frac{\mu - \rho}{4} U \end{bmatrix} < 0
\end{aligned}
\tag{16}
$$

The optimal AW compensator is computed as $D_{aw} = XU^{-1}$. The matrix Q, inverse of the Lyapunov stability matrix, characterizes the domain of attraction $\mathcal{E}(Q^{-1})$. The matrix Y controls the regionality of the solution: as $s \to \infty$, $Y \to 0$, making the local performance γ converge to the global level γ_G. Including Y as a free variable enables synthesis with regional guarantees, while a solution with γ independent of s ensures global guarantees. The final condition in Equation 16, the strong well-posedness constraint, prevents algebraic loops in the AW closed loop. It depends on two free parameters, ρ and μ, chosen to balance LMI feasibility with a small Lipschitz constant of the right-hand side. The selection is subject to $\mu > \rho > 1$ [33].

For the signal choice, d is the pitch acceleration disturbance, representing effects such as thrust vector misalignment, while the performance output z matches the plant outputs. The disturbance energy bound is set to $s = 100$. Well-posedness properties, relevant for static DLAW, are set to the minimum feasible values to reduce algebraic loop issues. MATLAB's LMILAB solver is used, and the resulting gains are shown in Table 3. It should be noted that such synthesis will be performed offline, rather than online during the vehicle's flight, to mitigate the risk of solvers not producing a meaningful solution. Similarly to regular controllers, the anti-windup compensators can be scheduled along different points in the flight envelope to cover a wider range of cases.

Table 3 Linear AW synthesis results

Architecture	γ	$\mathbf{D_{aw}}$
Anti-reset Windup	0.039	[-0.0118]
Static DLAW	0.039	[-0.0019 0.012 -0.2]

Notably, for one synthesis point, both architectures yield the same performance level γ when synthesized with the same parameter configuration. This indicates that the classical architecture should perform as well as static DLAW around this value of s. However, it is not a guarantee of performance for a larger range of values of s. A more extensive analysis on this matter is conducted in subsection 5.1.

4.7 LQ-Based Design

Tuning of the MRAW compensator follows the rationale of LQ-based design, where a quadratic performance index of weighted system states and inputs should be minimized. This variation of MRAW does not explicitly include characterization of saturation functions in the design, but rather uses an approximate model of the plant that does not include saturation effects. The closed-loop system P_{LQR} for LQ-based MRAW compensator synthesis is set up as in Equation 17.

$$\begin{cases} \dot{x}_{aw} = \bar{A}_p x_{aw} + \bar{B}_{pu} v + B_w w \\ z_{aw} = \begin{bmatrix} \sqrt{Q_P} \\ 0 \end{bmatrix} x_{aw} + \begin{bmatrix} 0 \\ \sqrt{R_P} \end{bmatrix} v \\ y = I_{n_p} x_{aw} \end{cases} \tag{17}$$

The system uses an online plant model, which allows for the use of full state feedback, as all the states are available by definition. The matrix B_w in this context represents the initial condition x_0, while $w(t)$ is taken as an impulse $\delta(t)$. Synthesizing the MRAW gains corresponds to finding a gain matrix K_{aw}. The Q_P matrix is defined as a diagonal matrix, with terms $Q_{x_i x_i}$, corresponding to respective states, on its diagonal. The matrix R_P consists of a single term R_{vv}, related to the penalty imposed on the signal v. The tuning is performed in MATLAB's `systune` framework, using the `TuningGoal.WeightedVariance` objective, according to Equation 18.

$$\left\| W_L(s) P_{LQR}(s) W_R(s) \right\|_2 < 1, \quad \text{with } W_L = I,\ W_R = \begin{bmatrix} \sqrt{Q_P} & 0 \\ 0 & \sqrt{R_P} \end{bmatrix} \tag{18}$$

For the selection of Q_P and R_P, one state to be regulated is chosen, namely the pitch angle θ, and the corresponding term $Q_{\theta\theta}$ is varied, while the other terms of Q_P are set to zero, and R_{vv} is set to identity. Notably, the synthesis is valid for the system P_{LQR}, which is an approximation of $\mathcal{P}_{cl}$ in the low saturation region. While literature has shown that such an approximation can be quite powerful, selecting an LQ-based MRAW compensator only with this analysis does not offer a stability guarantee akin to previous design.

5 Results

Methodologies of flight control design and AW augmentation have been used to synthesize a baseline controller and three distinct AW compensators. This section presents the results on performance and robustness of these schemes. The chosen simulation scenario considers the vehicle in a steady-state flight condition, and introduces a large disturbance on the pitch acceleration $\dot{q}$. Such a scenario is common within agile aerospace vehicle operations, and can be attributed to actuation faults, such as thrust vector misalignment. Before the time domain results, the $\mathcal{L}_2$ gain analysis of the AW schemes is carried out, to evaluate the robustness of the proposed schemes.

5.1 $\mathcal{L}_2$ Gain Analysis

The $\mathcal{L}_2$ gain from disturbance inputs to performance outputs is a tool to conservatively analyze the performance of a closed-loop system in the presence of saturation. To obtain more insight about the constrained system behavior, the performance level γ, which represents the $\mathcal{L}_2$ gain, can be computed for a range of values for parameter s, which bounds the energy of the disturbance signal. Such a curve, denoted by $\Gamma(s)$, is constructed by solving a set of LMIs, given by Equation 19, for a range of values of s.

$$
\begin{aligned}
&\Gamma(s) := \min_{Q,U,Y,\gamma} \gamma \quad \text{subject to} \\
&Q = Q^T > 0 \\
&U > 0 \\
&\mathrm{He}\begin{bmatrix} \mathcal{A}Q & \mathcal{B}_\phi U & \mathcal{B}_d & 0 \\ Y + C_y Q & \mathcal{D}_{y\phi} U - U & \mathcal{D}_{yd} & 0 \\ 0 & 0 & -\frac{I}{2} & 0 \\ C_z Q & \mathcal{D}_{z\phi} U & \mathcal{D}_{zd} & -\frac{\gamma^2 I}{2} \end{bmatrix} < 0 \\
&\begin{bmatrix} Q & Y^T \\ Y & \frac{\bar{u}^2}{s^2} \end{bmatrix} \geq 0
\end{aligned}
\tag{19}
$$

The closed-loop matrices originate from the plant and controller matrices, as defined in equations (13) and (10). The AW injection and compensator matrices depend on the specific AW scheme considered. This general formulation is applicable to all AW schemes discussed in this chapter, as well as to constrained systems without AW, enabling meaningful comparisons. All results in this section were obtained using MATLAB's LMILAB solver.

Each curve represents the $\Gamma(s)$ function from selected disturbance inputs to performance outputs. Since system variables like angles, rates, and accelerations differ in units and magnitudes, comparisons are limited to cases with the same signal types. The relevant range of the parameter s depends on the disturbance input type, as angle-based disturbances typically carry less energy than rate-based ones. The three AW compensator designs analyzed here correspond to the three methodologies introduced in this chapter.

1) **AR (green):** Anti-reset windup, classical AW scheme designed according to subsection 4.6
2) **DLAW (blue):** Static DLAW, designed according to subsection 4.6
3) **MRAW (orange):** LQ-based MRAW, designed according to subsection 4.7, with $Q_{\theta\theta} = 60$

The first $\mathcal{L}_2$ gain analysis can be conducted on the same set of disturbance inputs and performance, on which the AW compensator design was carried out, which are the pitch acceleration disturbance $d_{\dot{q}}$, and the plant outputs pitch angle θ and rate q. The two comparison of $\mathcal{L}_2$ gain curves are illustrated in Figure 6 for pitch rate output.

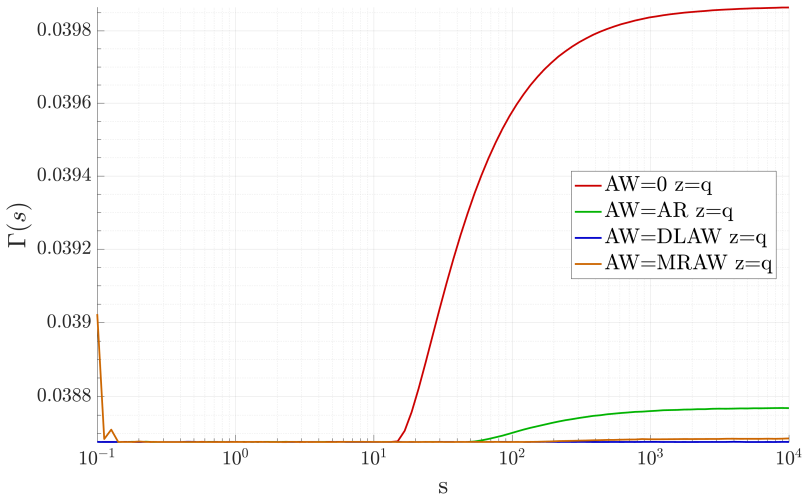

Fig. 6 $\mathcal{L}_2$ **gain curves from** $d_{\dot{q}}$ **to** q

The curve shapes match those in [20], confirming the analysis. All curves coincide for low s, representing the $\mathcal{L}_2$ gain in the linear domain where saturations and AW schemes are inactive. The linear

performance level is about 0.0387 for pitch rate. These low γ values arise because signal energy is expressed in angular acceleration units, which generally have higher magnitudes than angular velocity units. The curves plateau at different levels, with the DLAW scheme performing best, yielding an almost flat $\Gamma(s)$ and approaching a global performance guarantee. Anti-reset windup also outperforms the no-AW case, while the LQ-based MRAW reaches almost the same performance as DLAW.

5.2 Time Domain Simulations

All three AW schemes of AR (green), DLAW (blue), and MRAW (orange), are now evaluated in the time domain, against a baseline case with no AW compensation (dotted-black). The results for pitch angle, actuator magnitude and rate, are shown in Figure 7. The main features of the simulation setup can be summarized as follows:

- The plant model used is the one introduced in section 2, with the nonlinear actuator of subsection 2.3, introducing limits on actuator magnitude, rate, and acceleration
- All models use the same baseline controller synthesized in section 3
- Anti-Windup compensators are driven by the rate saturation model of Figure 2. This introduces an assumption that the actual saturation level of the actuator is known by the controller, which may not always be accurate and depends on the actuator hardware
- The simulation assumes a vehicle initially in a steady-state flight condition, and introduces a high-magnitude pitch acceleration disturbance, which can be associated with actuator faults, such as thrust vector misalignment

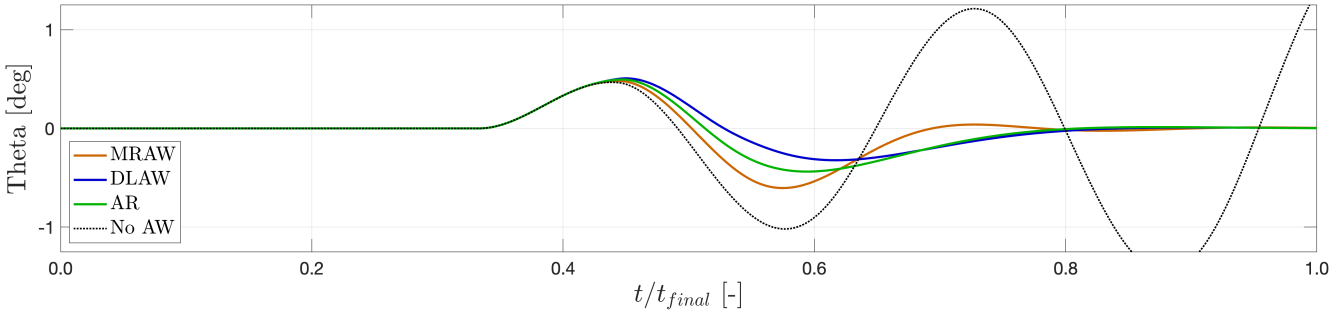

(a) Pitch angle and reference signal time evolution

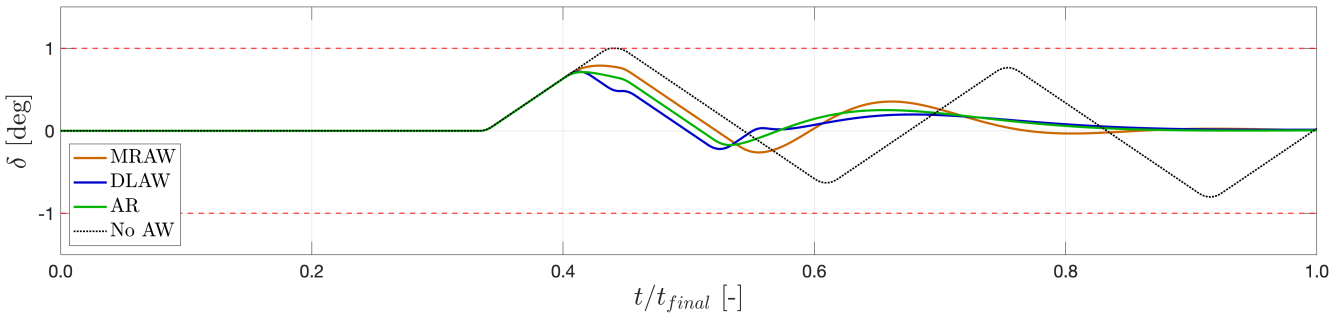

(b) Actuator magnitude time evolution

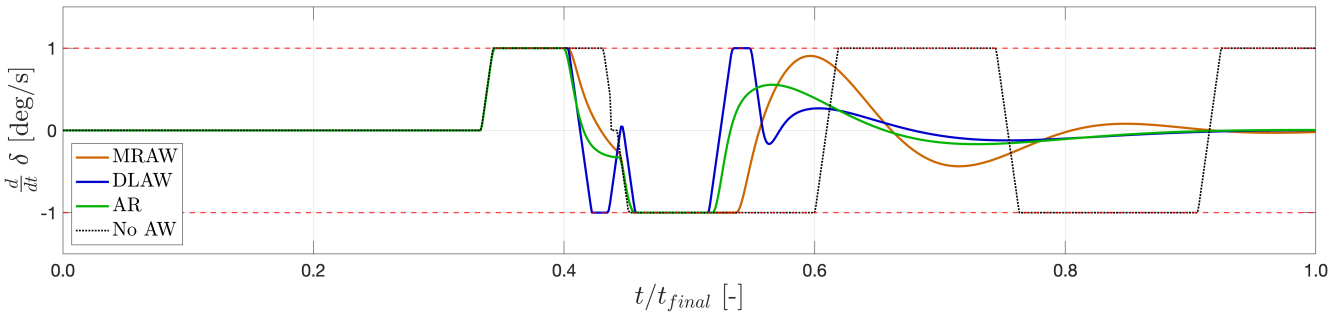

(c) Actuator rate time evolution

Fig. 7 Simulation results comparing performance of various AW schemes against a setup with no AW augmentation

The pitch acceleration disturbance, which caused severe performance degradation for the linear controller without AW augmentation, is rejected well by all three AW schemes. The classical anti-reset windup performs very well, despite having a much simpler structure. The trajectory of control action and plant outputs for DLAW and AR is very similar, although additional corrective actions can be seen in actuator rate, in Figure 7c. They can be attributed to the additional signals introduced by static DLAW. LQ-based MRAW exhibits a more aggressive control action, which results in slightly faster pitch angle recovery, at the expense of a higher pitch rate.

6 Conclusions

This work has studied a control problem for agile aerospace vehicle application, in the presence of multiple saturations. CLS signal-based design has been applied to synthesize a baseline controller of a pre-defined structure, exhibiting good performance and robustness qualities in the linear domain. Despite the good stability margins and time-domain responses, the baseline controller's performance severely degraded in the presence of saturations. Three distinct anti-windup schemes were proposed as a controller augmentation, and their performance compared. To accommodate anti-windup compensation driven by rate saturation signal, a model similar to [27] was implemented, where an augmented plant and controller are constructed to isolate the rate saturation block, which is used to drive the AW compensators. It was found to be a suitable extension to allow for rate saturation AW design for a non-strictly proper controller outputting a magnitude signal. The three AW schemes, anti-reset windup, static DLAW and LQ-based MRAW, have all shown significant improvement in the disturbance rejection simulation scenario, with the MRAW scheme exhibiting the largest design freedom. A comparative analysis of $\mathcal{L}_2$ gain of the AW schemes was carried out, which showcased the best $\mathcal{L}_2$ gain bounds for the DLAW scheme. This has indicated that the $\mathcal{L}_2$ gain is a valid metric for AW design, but should not be used in isolation.

A number of future studies can build upon this work. Firstly, the modeling aspect can be extended to bring the analysis closer to a realistic experimental setup. Nonlinear airframe dynamics could be included, as well as an extended actuator model accounting for the hardware components responsible for the saturation limits. The analysis can also be carried out over the whole flight envelope. Reaching further, the simulations could be realized in an experimental setup using a test-bench with real, electro-mechanical or hydraulic actuators. This could uncover the potential mismatch of the actual saturation limits in operational conditions, compared to the limits used internally by the controller. Evaluating this aspect in more detail could extend the knowledge about sensitivity of the anti-windup to such modeling uncertainties.

7 Declaration of Use of Artificial Intelligence

Artificial Intelligence was not used in the work presented.

References

[1] Pierre Apkarian and Dominikus Noll. Nonsmooth H∞ synthesis. *IEEE Transactions on Automatic Control*, 51(1):71–86, 1 2006. ISSN: 00189286. doi: 10.1109/TAC.2005.860290.

[2] P Apkarian and Dominikus Noll. The H∞ Control Problem is Solved. 2017. doi: 10.12762/2017.AL13-01ï.

[3] Seonhyeok Kang, H. Jin Kim, Jin Ik Lee, Byung Eul Jun, and Min Jea Tahk. Roll-pitch-yaw integrated robust autopilot design for a high angle-of-attack missile. *Journal of Guidance, Control, and Dynamics*, 32(5):1622–1628, 2009. ISSN: 15333884. doi: 10.2514/1.39812.

[4] Jong Han Kim and Ick Ho Whang. Augmented three-loop autopilot structure based on mixed-sensitivity h∞ optimization. *Journal of Guidance, Control, and Dynamics*, 41(3):748–753, 2018. ISSN: 15333884. doi: 10.2514/1.G003119.

[5] Spilios Theodoulis, Florian Sève, and Philippe Wernert. Robust gain-scheduled autopilot design for spin-stabilized projectiles with a course-correction fuze. *Aerospace Science and Technology*, 42:477 – 489, 4 2015. ISSN: 12709638. doi: 10.1016/j.ast.2014.12.027.

[6] Swapnil Pramod Kanade and Abraham T Mathew. 2 DOF H- Infinity Loop Shaping Robust Control for Rocket Attitude Stabilization. *International Journal of Aerospace Sciences*, 2(3):71–91, 2013. ISSN: 2169-8899. doi: 10.5923/J.AEROSPACE.20130203.02.

[7] Arshad Mahmood, Yoonsoo Kim, and Jeongho Park. Robust H∞ autopilot design for agile missile with time-varying parameters. *IEEE Transactions on Aerospace and Electronic Systems*, 50(4):3082 – 3089, 10 2014. ISSN: 00189251. doi: 10.1109/TAES.2014.130750.

[8] Spilios Theodoulis and Gilles Duc. Missile autopilot design: Gain-Scheduling and the gap metric. *Journal of Guidance, Control, and Dynamics*, 32(3):986–996, 2009. ISSN: 15333884. doi: 10.2514/1.34756.

[9] Spilios Theodoulis, Michael Proff, and Charlotte Marchand. Robust Design for Highly Agile Missile Autopilots. *Mediterranean Conference on Control and Automation*, page 1109, 2020. doi: 10.1109/MED48518.2020.9183304.

[10] Spilios Theodoulis and Michael Proff. Robust flight control tuning for highly agile missiles. In *AIAA Scitech 2021 Forum*, pages 1–26. American Institute of Aeronautics and Astronautics Inc, AIAA, 2021. ISBN: 9781624106095. doi: 10.2514/6.2021-1568.

[11] Mayuresh V. Kothare, Peter J. Campo, Manfred Morari, and Carl N. Nett. A unified framework for the study of anti-windup designs. *Automatica*, 30(12):1869 – 1883, 12 1994. ISSN: 00051098. doi: 10.1016/0005-1098(94)90048-5.

[12] João Manoel Gomes da Silva and Sophie Tarbouriech. Antiwindup design with guaranteed regions of stability: An LMI-based approach. *IEEE Transactions on Automatic Control*, 50(1):106–111, 1 2005. ISSN: 00189286. doi: 10.1109/TAC.2004.841128.

[13] Tingshu Hu, Andrew R. Teel, and Luca Zaccarian. Nonlinear L2 gain and regional analysis for linear systems with anti-windup compensation. In *Proceedings of the American Control Conference*, volume 5, pages 3391–3396, 2005. doi: 10.1109/acc.2005.1470495.

[14] Nobutaka Wada and Masami Saeki. Synthesis of a Static Anti-Windup Compensator for Systems with Magnitude and Rate Limited Actuators. 2000. doi: 10.1016/S1474-6670(17)36217-1.

[15] Fen Wu and Marco Soto. Extended anti-windup control schemes for LTI and LFT systems with actuator saturations. *International Journal of Robust and Nonlinear Control*, 14(15):1255–1281, 10 2004. ISSN: 10498923. doi: 10.1002/rnc.943.

[16] Andrew Teel and Navneet Kapoor. *The L2 Anti-windup problem: Its definition and solution*. 1997. ISBN: 9783952426906.

[17] Luca Zaccarian and Andrew R. Teel. A common framework for anti-windup, bumpless transfer and reliable designs. *Automatica*, 38(10):1735–1744, 10 2002. ISSN: 0005-1098. doi: 10.1016/S0005-1098(02)00072-9.

[18] Fulvio Forni, Sergio Galeani, and Luca Zaccarian. Model Recovery Anti-Windup for Plants with Rate and Magnitude Saturations. 2009. doi: 10.23919/ECC.2009.7074422.

[19] Sergio Galeani, Sophie Tarbouriech, Matthew Turner, and Luca Zaccarian. A tutorial on modern anti-windup design. *European Journal of Control*, 15(3-4):418–440, 2009. ISSN: 09473580. doi: 10.3166/EJC.15.418-440.

[20] Luca Zaccarian and Andrew R. Teel. *Modern anti-windup synthesis: control augmentation for actuator saturation*. Princeton University Press, 2011. ISBN: 9780691147321.

[21] Sophie Tarbouriech, Germain Garcia, João Manoel Gomes da Silva, and Isabelle Queinnec. *Stability and Stabilization of Linear Systems with Saturating Actuators*. Springer London, 2011. doi: 10.1007/978-0-85729-941-3.

[22] Sovanna Thai. Robust gain-scheduled autopilot design with anti-windup compensation for a guided projectile. *CEAS Aeronautical Journal*, 14(3):765–786, 7 2023. ISSN: 18695590. doi: 10.1007/s13272-023-00668-9.

[23] Sovanna Thai. *Advanced anti-windup flight control algorithms for fast time-varying aerospace systems*. PhD thesis, ISAE-SUPAERO, 2022.

[24] Lars Rundqwist and Karin Stihl-Gunnarsson. Phase Compensation of Rate Limiters in Unstable Aircraft. 1996. doi: 10.1109/CCA.1996.558586.

[25] Sarah L. Gatley, Matthew C. Turner, Ian Postlethwaite, and Abhishek Kumar. A comparison of rate-limit compensation schemes for pilot-induced- oscillation avoidance. *Aerospace Science and Technology*, 10(1):37–47, 1 2006. ISSN: 12709638. doi: 10.1016/j.ast.2005.07.004.

[26] Sergio Galeani, Simona Onori, Andrew R Teel, and Luca Zaccarian. Further results on static linear anti-windup design for control systems subject to magnitude and rate saturation. 2006. doi: 10.1109/CDC.2006.377819.

[27] S. Galeani, S. Onori, A. R. Teel, and L. Zaccarian. A magnitude and rate saturation model and its use in the solution of a static anti-windup problem. *Systems and Control Letters*, 57(1):1–9, 1 2008. ISSN: 01676911. doi: 10.1016/j.sysconle.2007.06.011.

[28] Jean-Marc Biannic and Sophie Tarbouriech. Stability and Performance Enhancment of a Fighter Aircraft Flight Control System by a New Anti-Windup Approach. 2007. doi: 10.3182/20070625-5-FR-2916.00031.

[29] J. M. Gomes da Silva, Eduardo Limon, T. Alamo, and E. F. Camacho. Dynamic output feedback for discrete-time systems under amplitude and rate actuator constraints. *IEEE Transactions on Automatic Control*, 53(10):2367–2372, 2008. ISSN: 00189286. doi: 10.1109/TAC.2008.2007521.

[30] Fernando Augusto Bender and João Manoel Gomes da Silva Jr. Acceleration-bounded Control for Discrete Time Linear Systems. 2007. doi: 10.3182/20071017-3-BR-2923.00082.

[31] Carlos Alcolea Pérez, Spilios Theodoulis, Florian Sève, and Laurent Goerig. Automatic weighting filter tuning for robust flight control law design. In *IFAC-PapersOnLine*, volume 55, pages 400–405. Elsevier B.V., 7 2022. doi: 10.1016/j.ifacol.2022.09.057.

[32] Yu Huang, Timo Pe, Andrey P. Popov, Herbert Werner, and Frank Thielecke. Control of a two-load-path trimmable horizontal stabilizer actuator of an aircraft - Comparison of H∞ design approaches. *Proceedings of the IEEE Conference on Decision and Control*, pages 4863–4868, 2010. ISSN: 25762370. doi: 10.1109/CDC.2010.5716948.

[33] Gene Grimm, Andrew R Teel, and Luca Zaccarian. Establishing Lipschitz properties of multivariable algebraic loops with incremental sector nonlinearities. 2003. doi: 10.1109/CDC.2003.1271907.

A Additional Matrix Definitions

This appendix presents some additional definitions of the matrices introduced in the main body of the paper. It is meant as a complimentary material as the most important definitions are included in the main body.

Equation 20 presents the matrices defining the controller $K(s)$ in terms of the control gains.

$$\left[\begin{array}{c|c|c} A_c & B_{cu} & B_{cr} \\ \hline C_c & D_{cu} & D_{cr} \end{array}\right] = \left[\begin{array}{c|cc|c} 0 & -1 & 0 & 1 \\ \hline K_i & K_\theta & K_q & K_{ff} \end{array}\right] \tag{20}$$

Equation 21 shows the closed-loop matrices of the linear system P_{cl} in terms of plant and controller matrices.

$$\left[\begin{array}{c|c|c} \mathbf{A} & \mathbf{B_d} & \mathbf{B_r} \\ \hline \mathbf{C_z} & \mathbf{D_{zd}} & \mathbf{D_{zr}} \\ \hline \mathbf{C_y} & \mathbf{D_{yd}} & \mathbf{D_{yr}} \end{array}\right] = \left[\begin{array}{cc|c|c} A_p + B_{pu}D_{cu}C_p & B_{pu}C_c & B_{pd} + D_{pd}D_{cu}B_{pu} & D_{cr}B_{pu} \\ B_{cu}C_p & A_c & D_{pd}B_{cu} & B_{cr} \\ \hline C_p & 0 & D_{pd} & 0 \\ \hline D_{cu}C_p & C_c & D_{cu}D_{pd} & D_{cr} \end{array}\right] \tag{21}$$

Equation 22 presents the matrices of the augmented controller $\mathscr{K}(s)$ in terms of control gains and the rate saturation model parameters c and K.

$$\left[\begin{array}{c|c|c} \bar{A}_c & \bar{B}_{cu} & \bar{B}_{cr} \\ \hline \bar{C}_c & \bar{D}_{cu} & \bar{D}_{cr} \end{array}\right] = \left[\begin{array}{cc|ccc|c} 0 & 0 & -1 & 0 & 0 & 1 \\ K_i & -\frac{1}{c} & K_\theta & K_q & 0 & K_{ff} \\ \hline \left(\frac{1}{c}+K\right)k_i & -\frac{1}{c^2} & \left(\frac{1}{c}+K\right)k_\theta & \left(\frac{1}{c}+K\right)k_q & -K & \left(\frac{1}{c}+K\right)k_{ff} \end{array}\right] \tag{22}$$